



Effects of polyethylene glycol and gelatin on the crystal size, morphology, and Sn^{2+} -sensing ability of bismuth deposits

Yi-Da Tsai², Chein-Hung Lien², Chi-Chang Hu^{*,1}

Department of Chemical Engineering, National Tsing Hua University, Hsin-Chu 30013, Taiwan

ARTICLE INFO

Article history:

Received 28 January 2011

Received in revised form 27 May 2011

Accepted 25 June 2011

Available online 1 July 2011

Keywords:

Bi sensor

Electrodeposition

Complex agent

Linear sweep voltammetry

Square-wave anodic stripping voltammetry

ABSTRACT

The influences of citric acid (CA), ethylenediaminetetraacetic acid (EDTA), polyethylene glycol (PEG), and gelatin on the deposition behavior of Bi were systematically investigated through the linear sweep voltammetric (LSV) analysis. Based on the LSV results, deposits plated from a typical solution containing 0.05 M $\text{Bi}(\text{NO}_3)_3 \cdot 5\text{H}_2\text{O}$ and various combinations of complex agents and additives with pH = 3.5 at 1 and 30 mA cm^{-2} were characterized by scanning electron microscopic (SEM) and X-ray diffraction (XRD) analyses. The adhesion of deposits and the formation of dendrites were respectively improved and inhibited by the adsorption of PEG onto Bi deposits. With adding the above four compounds, a synergistic effect was shown to reach a nano-sized, sphere-like, porous morphology of a Bi deposit at 30 mA cm^{-2} . The crystal size and morphology of Bi deposits were found to affect the sensing ability of Sn^{2+} through the square-wave anodic stripping voltammetric (SWASV) analysis.

© 2011 Elsevier Ltd. All rights reserved.

1. Introduction

Recently, increased attention on the electrochemical deposition of bismuth has been paid for the electrochemical community, due to the unique electrical and physicochemical properties of bismuth for several applications [1–6], especially in developing the heavy metal sensors [7,8]. For instance, an extremely high magneto-resistance effect has been observed earlier in the Bi single-crystals, thin films, and nanowires, leading Bi to be a promising material of the magnetic sensor. In addition, bismuth is an environment friendly element with a low toxicity, which has been used widely in the pharmaceutical industry [1]. Besides, bismuth film electrodes (BFEs) were proposed for the cathodic detection of organic compounds and metallic ions [2], the anticorrosive interlayer in batteries [3], magnetic field [4], current sensors [5], and decorative coatings due to the excellent hydrogen embitterment inhibition of Bi coatings [6]. Traditionally, determination of metals or heavy metals was extensively carried out at mercury-film electrodes (MFEs) by means of the anodic stripping voltammetric analysis, due to the advantages of high sensitivity, reproducibility, and high hydrogen evolution overpotential, etc. [7,8]. However, because of its toxicity to human health and the damages to our environment, mercury-based electrodes must be restricted. Consequently, BFEs, one kind

of the mercury-free electrodes with environmental friendly properties, which are comparable to MFEs, have been proposed to replace MFEs for the application of sensors.

In general, BFEs can be fabricated by several methods, such as thermal evaporation [9], electrodeposition [10,11], DC sputtering [12], RF magnetron sputtering [13], and molecular beam epitaxy [14]. Among these methods, electrodeposition is a simple route to control the surface morphologies of the coatings via changing the electroplating solutions such as composition, complex agents, additives, pH, and temperature, as well as the deposition parameters e.g., current density and applied potential [15–17]. Moreover, it offers other merits, including a high deposition rate, mass productivity, industrially well-established technology, cost-effectivity, etc. Hence, electrodeposition has been progressively recognized as a popular technology for the coating application. On the other hand, little literature has been published on how to control the morphology and adhesion of Bi deposits through electroplating [10,11], probably due to the instability of free Bi^{3+} ions. Accordingly, one of the purposes in this study is to control the morphology and crystal size of Bi deposits through electroplating under a DC mode by adding organic agents in various combinations into the plating solution.

In this work, the influences of citric acid (CA), ethylenediaminetetraacetic acid (EDTA), polyethylene glycol (PEG), and gelatin on the deposition behavior of Bi were systematically investigated through the linear sweep voltammetric (LSV) analysis. Based on the LSV results, Bi deposits were electroplated from the bath containing different combinations of complex agents and additives. The morphologies and crystalline structure of resultant deposits

* Corresponding author. Tel.: +886 3 5736027; fax: +886 3 5736027.

E-mail address: cchu@che.nthu.edu.tw (C.-C. Hu).

¹ ISE Member.

² Both the authors contributed equally to this work.

Table 1
The bath composition and plating conditions of Bi deposition.

Bi(NO ₃) ₃ ·5H ₂ O	0.05	M
Citric acid (CA)	0.3	M
Ethylenediaminetetraacetic acid (EDTA)	0.3	M
Polyethylene glycols (PEG, MW 400)	0.2	M
Gelatin	4000	ppm
Current density	1 or 30	mA cm ⁻²
Temperature	25	°C
pH	3.5	

were characterized by means of scanning electron microscopic (SEM) and X-ray diffraction (XRD) analyses, respectively. Finally, the sensitivity of five typical BFEs on Sn(II) is evaluated by using the square-wave anodic stripping voltammetry (SWASV) method. In fact, the LSV responses of Bi deposition from the plating solutions containing CA, EDTA, and PEG have been preliminarily investigated in our previous studies for Sn–Bi alloy deposition [15,17]. However, the effects of these organic agents in addition to gelatin on the Bi deposition behavior in previous baths are not directly applicable to this study because of the significant differences in pH values among these plating baths.

2. Experimental

Bismuth deposits were electroplated from a simple solution onto copper (99.5%, 1.094 × 10⁻² cm², 1.18 × 10⁻¹ cm in diameter) circular plates which have been deposited with a nickel film (ca. 2 μm). The pretreatment procedures of Cu/Ni substrates completely followed our previous work [15–19]. The Cu/Ni substrates, rinsed with deionized water, were vertically placed in a 100-ml jacket cell surrounded with a dimensionally stable anode (DSA[®], an (Ru–Ti)O₂-coated Ti electrode). All substrates were electroplated with Bi deposits with a constant passed charge density (0.09 C cm⁻²) for the textural analyses and the Sn²⁺-sensing tests. The basic plating bath, shown in Table 1, consisted of 0.05 M Bi(NO₃)₃·5H₂O (Hayashi, EP) and various complex agents or additives, including citric acid (CA, Shimakyu, EP), ethylenediaminetetraacetic acid (EDTA, Riedel-deHaen, GA), polyethylene glycols (PEG 400, MW 400, Shimakyu, EP), and gelatin (from porcine skin, Type A~300 Bloom (G2500-100G)) in various combinations. The pH of plating baths was adjusted to be 3.5 with concentrated HCl or NH₄OH. The plating baths were not agitated during the DC electroplating of Bi. After deposition, these electrodes were repeatedly rinsed with deionized water and finally dried in a vacuum oven at room temperature. The thickness of Bi deposits, significantly influenced by the combination of organic agents employed in this work, is between 3.9 and 0.5 μm although a constant passed charge density (0.09 C cm⁻²) is employed.

The electrochemical analyses were performed with an electrochemical analyzer system, CHI 660c (CH Instruments, USA). All electrochemical analyses were carried out in a three-compartment cell. An Ag/AgCl electrode (Argenthal, 3 M KCl, 0.207 V versus a standard hydrogen electrode (SHE) at 25 °C) was utilized as the reference electrode and a piece of platinum gauze with an exposed area equal to 4 cm² served as the counter electrode. A Luggin capillary, whose tip was set at a distance of 1–2 mm from the surface of substrates, was used to minimize errors due to *iR* drop in the electrolytes. For the SWASV measurements, the testing solutions contain 0.1 M CA (Shimakyu, EP) and SnCl₂·nH₂O (Hayashi, EP) in various concentrations. The concentrations of dissolved Sn(II) ions have been confirmed by an inductively coupled plasma-mass spectrometer (ICP-MS, SCIEX ELAN 5000). The cathodic deposition for accumulating Sn onto the BFEs was fixed at –0.8 V for 300 s under a magnetic stirring rate of 100 rpm. The Sn-coated BFEs rinsed with deionized water were anodically stripped in a 0.1 M CA solu-

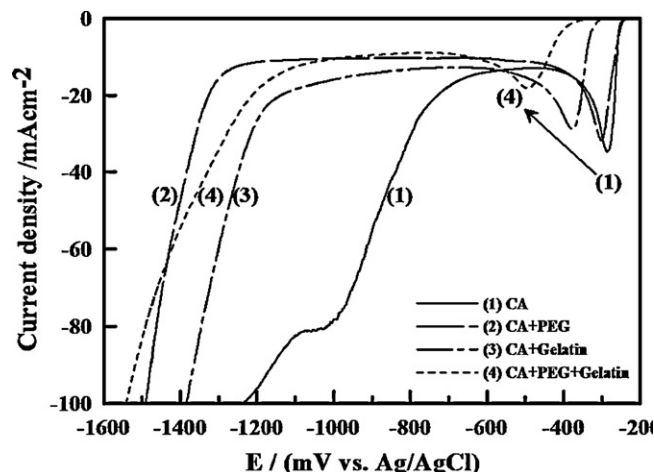


Fig. 1. LSV curves measured from the plating solution containing 0.05 M Bi³⁺ with (1) 0.3 M CA, (2) 0.3 M CA + 0.2 M PEG, (3) 0.3 M CA + 4000 ppm gelatin, and (4) 0.3 M CA + 0.2 M PEG + 4000 ppm gelatin onto the Cu/Ni electrode. LSV curves were measured at 8 mV s⁻¹ and 25 °C.

tion (pH = 2) without stirring. The SWASV curves were recorded between –0.6 and –0.3 V at an applied frequency of 15 Hz with the amplitude of 25 mV and a potential step of 4 mV.

Morphologies of all deposits were examined by a field emission scanning electron microscope (FE-SEM, Hitachi S-4700). X-ray diffraction patterns were obtained from an X-ray diffractometer (CuK α , Ultima IV, Rigaku).

All solutions were prepared with deionized water produced by a reagent water system (Milli-Q SP, Japan) at 18 M Ω cm and all reagents not specified were Merck, GR. The solutions for the LSV and SWASV analyses were degassed with purified nitrogen gas for 20 min before the electrochemical measurements and nitrogen was passed over the solution during the measurements. Solution temperature was maintained at the specified temperature with an accuracy of 0.1 °C by means of a water thermostat (Haake DC3 and K20).

3. Results and discussion

3.1. Linear sweep voltammetric study

Curves 1–4 in Fig. 1 show the influences of PEG and gelatin on the deposition behavior of Bi on the Cu/Ni substrate in the solution containing 0.05 M Bi³⁺ and 0.3 M CA. On curve 1, Bi deposition commences at ca. –240 mV with an obvious peak centered at ca. –280 mV, attributable to the deposition of free Bi³⁺ with a limiting current density of 12 mA cm⁻² from –400 and –600 mV. The shoulder wave at ca. –1000 mV may correspond to the Bi deposition from the Bi³⁺–CA complex species, indicating a weak complex agent of citrate for Bi³⁺ [15,17]. The increase in the current density at potentials negative to –600 mV is attributed to the hydrogen evolution reaction (HER). On curve 2, the limiting current density (ca. 10 mA cm⁻²) of free Bi³⁺ deposition continues to –1200 mV, suggesting a leveling effect of this strongly adsorbed PEG, leading to a uniform deposit [17,20]. The above different *i*–*E* responses at potentials negative to –400 mV are attributed to the PEG adsorption on Bi already deposited, inhibiting the deposition of Bi³⁺–CA complex species. On the other hand, the sharp increase in the hydrogen evolving currents behind –1400 mV implies the potential-dependent desorption of PEG on Bi and Cu/Ni substrate in this potential region [21]. On curve 3, gelatin is considered as a leveling agent due to its strong adsorption ability [22] and a complex agent coordinated with metallic ions [22,23]. The similar *i*–*E* responses of curves 1 and 3 at potentials positive to –600 mV sug-

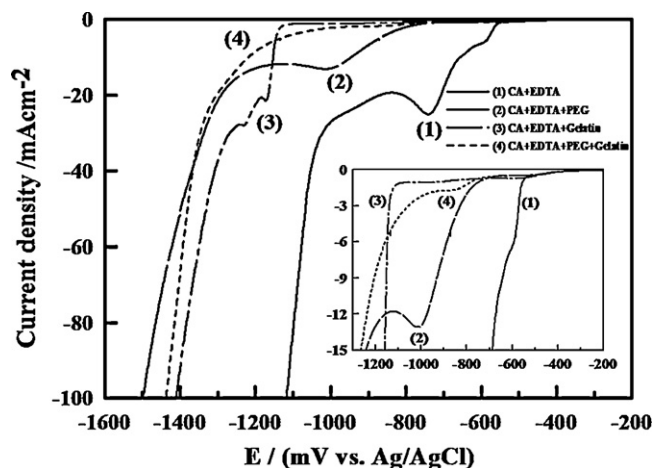


Fig. 2. LSV curves measured from the plating solution containing 0.05 M Bi^{3+} and 0.3 M EDTA with (1) 0.3 M CA, (2) 0.3 M CA+0.2 M PEG, (3) 0.3 M CA+4000 ppm gelatin, and (4) 0.3 M CA+0.2 M PEG+4000 ppm gelatin onto the Cu/Ni electrode. LSV curves were measured at 8 mV s^{-1} and 25°C .

gest that gelatin is a weak complex agent for Bi^{3+} . The relatively higher limiting current density, ca. 15 mA cm^{-2} between -600 and -1200 mV , suggests weaker adsorption strength of gelatin in comparing with PEG.

Curve 4 in Fig. 1 demonstrates the synergistic effect of the simultaneous addition of 0.3 M CA, 0.2 M PEG, and 4000 ppm gelatin into the electroplating bath. Here, gelatin, a polypeptide with high molecular mass, may form microspheres, adheres together, and displays a poor flow property in the gelatin–water system. Hence, gelatin usually acts as a film-forming polymer/surfactant to control the surface tension, which promotes the emulsification in the photographic industry [24]. However, the addition of PEG into the gelatin–water solution avoids this gathering phenomenon among the gelatin microdrops in the internal phase of emulsion by electrostatic and hydrophobic forces [25]. Thus, PEG works as a physical barrier for the aggregation of gelatin microspheres. As a result, some new micro-sized PEG–gelatin species should co-work to form a thin layer adsorbed onto the substrate/deposit surface [24,26]. Hence, curve 4 shows a negative shift in the onset potential to ca. -380 mV , a lower deposition rate (peak current $\approx 17 \text{ mA cm}^{-2}$), and the lowest limiting current density among all baths. This result implies the formation of a relatively stable metallic complex species, Bi^{3+} –PEG–gelatin.

Curves 1–4 in Fig. 2 show the effects of PEG and gelatin on the Bi deposition behavior measured from a bath containing 0.05 M Bi^{3+} + 0.3 M CA + 0.3 M EDTA. A comparison of curve 1 in Figs. 1 and 2 reveals that EDTA in the electroplating bath not only causes a negative shift in the onset potential of Bi deposition from -240 to -550 mV but also clearly reduces the peak current density of Bi deposition, indicative of relatively strong coordination between Bi^{3+} and EDTA. This result, similar to that measured from a Bi^{3+} solution at $\text{pH} = 2$ or 6 , indicates that combination of CA and EDTA can significantly coordinate with Bi^{3+} [15–17]. Note the presence of a shoulder and a peak on curve 1, suggesting that the concentration of EDTA is not sufficient to form stable Bi^{3+} –EDTA complex species. Thus, much more polarizable behavior of Bi deposition is obtained on curve 2 in Fig. 2. Clearly, the significant negative shift in the deposition potential and a much lower peak current density can be achieved by the coexistence of CA, EDTA, and PEG, revealing a synergistic effect on suppressing the deposition rate of Bi (in comparing with curve 2 in Fig. 1 and curve 1 in Fig. 2), similar to curve 4 in Fig. 1.

On curve 3, no significant current is found at potentials positive to ca. -1150 mV , indicating a nearly complete shielding effect of

this organic combination on the Bi deposition and HER. Two unobvious peaks around -1170 and -1230 mV may be due to the different deposition potentials of Bi^{3+} –EDTA complexes in various structures when gelatin leaves the substrate at ca. -1150 mV . Since Bi deposition and HER occur in the same potential region, gelatin should mainly act as an adsorption additive in plating Bi due to the strong coordination between Bi^{3+} and EDTA. A similar phenomenon is also visible for adding PEG into this bath (curve 2) while the shielding effect of gelatin on Bi deposition and HER is much stronger and more complete than that of PEG, judged from the more negative onset potential of Bi deposition and the double-layer-charging response at potentials above -1150 mV on curve 3. Thus, a stronger synergistic effect on suppressing the Bi deposition is obtained for this organic combination. On curve 4, Bi deposition commences at ca. -700 mV (based on 0.5 mA cm^{-2}), a potential very close to that on curve 2, but a much smaller plateau (1.7 mA cm^{-2}) is obtained at about -850 mV . This plateau may correspond to the same reaction in the peak centered at -1000 mV on curve 2. Therefore, the unchanged deposition potential of Bi^{3+} –EDTA but a lower current density indicates a significant suppression in the Bi deposition rate through adding gelatin into the CA + EDTA + PEG solution.

3.2. Textural analyses

Based on the LSV analyses, the crystal size and morphology of Bi deposits can be controlled by changing the combination of complex agents and additives. Figs. 3 and 4 show the SEM morphologies of Bi deposits (at 5000 and 200,000 magnifications, respectively) plated from the baths containing various combinations of complex agents/additives at two current densities. The adhesion, testing by ultrasonic vibration, of these deposits on the Cu/Ni substrate is shown in Table 2. From an examination of all SEM images, several distinct morphologies were obtained, which are strongly dependent on the composition of plating baths and the current density of deposition. In Figs. 3a, e and 4a, e, both Bi deposits show dendrite-like morphologies when the current density is 30 mA cm^{-2} . The adhesion of both deposits is very poor (see Table 2), indicating that the deposition rate at 30 mA cm^{-2} is too high. When a current density of 1 mA cm^{-2} is applied, the deposit plated from the bath containing both CA and EDTA shows a relatively compact morphology with good adhesion. Under such a deposition current density, the stacking of Bi atoms belongs to the pyramidal growth, indicating a steady growth of Bi crystals [27,28]. However, the Bi deposit plated from the solution containing CA only shows the dendrite morphology with poor adhesion although the current density is 1 mA cm^{-2} . Due to the rapid nucleation of Bi clusters, dendrites are easily obtained for a Bi deposit plated from a simple bath containing Bi^{3+} only [10,15,17,29]. Thus, CA, a weak complex agent for Bi^{3+} , cannot form stable Bi^{3+} –CA species in the plating bath at $\text{pH} = 3.5$ to reduce the nucleation rate of Bi [15]. The above difference suggests that the strong coordination between EDTA and Bi^{3+} not only negatively shifts the onset deposition potential but also reduce the nucleation rate of Bi clusters.

From Fig. 3b, the Bi deposit plated from the solution containing CA and PEG is piled with many grains without obvious dendrites. Under a high magnification (see Fig. 4b), these grains are composed of short rods and screw dislocations, indicating the enrichment of imperfections while this deposit shows excellent adhesion on the substrate. Besides, the deposits plated at 1 or 30 mA cm^{-2} show a similar morphology, indicating steady growth and nucleation of Bi grains although the HER occurs significantly at 30 mA cm^{-2} . From a comparison of Fig. 3a and b (or Fig. 4a and b), the relatively compact, polycrystalline, smooth morphology without dendrites reveals the significant improvement in the physical properties of resultant deposits with good adhesion, due to the strong adsorption of PEG on the deposit [15]. In Figs. 3f and 4f, the Bi deposit shows a branch-like

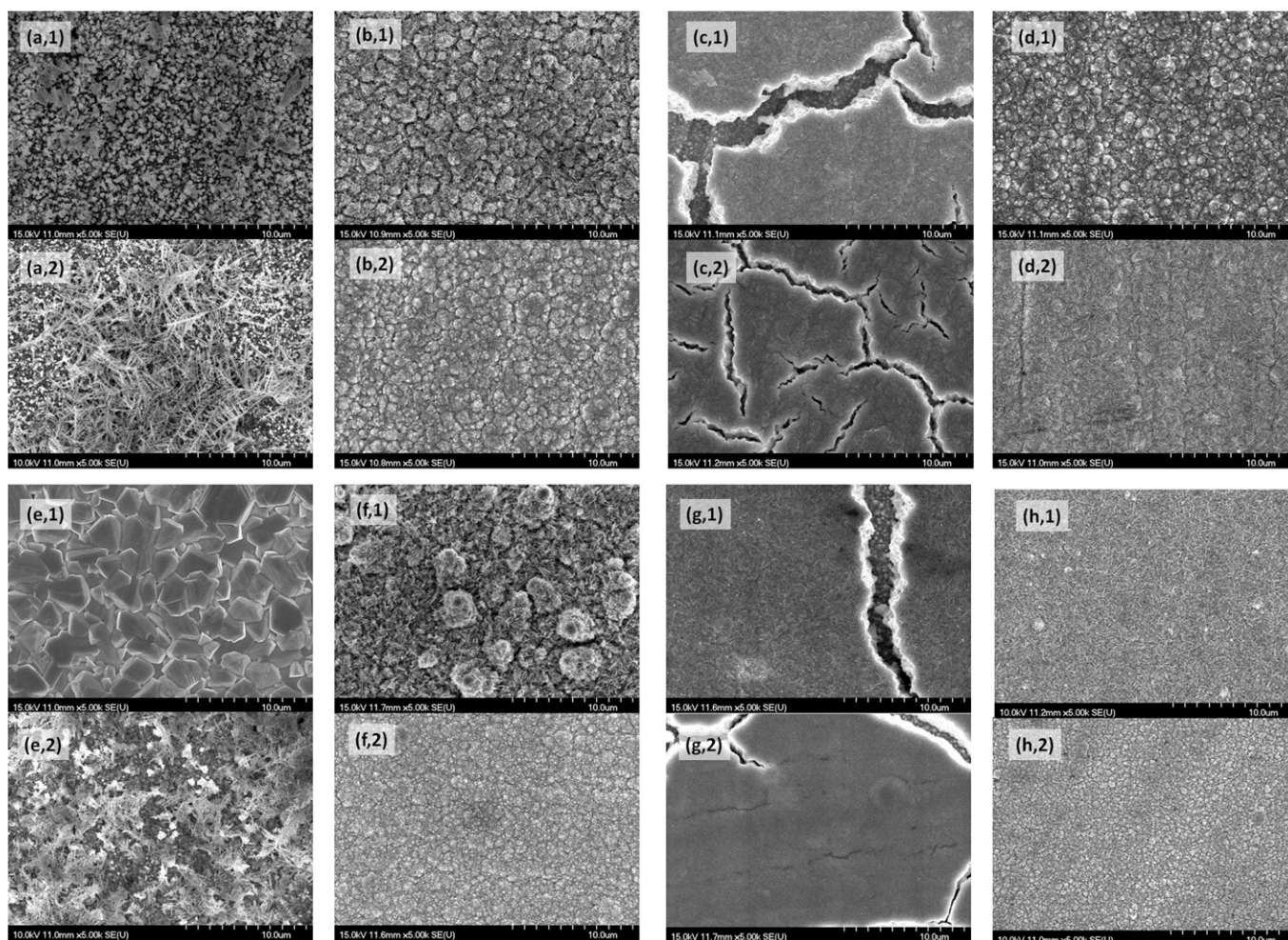


Fig. 3. SEM morphologies under a magnification of 5000 for Bi deposits plated at (1) 1 and (2) 30 mA cm⁻² from the basic plating bath (0.05 M Bi(NO₃)₃) with (a) 0.3 M CA, (b) 0.3 M CA + 0.2 M PEG, (c) 0.3 M CA + 4000 ppm gelatin, (d) 0.3 M CA + 0.2 M PEG + 4000 ppm gelatin, (e) 0.3 M CA + 0.3 M EDTA, (f) 0.3 M CA + 0.3 M EDTA + 0.2 M PEG, (g) 0.3 M CA + 0.3 M EDTA + 4000 ppm gelatin, and (h) 0.3 M CA + 0.3 M EDTA + 0.2 M PEG + 4000 ppm gelatin.

morphology enriched with thin skeletons when the applied current density is 1 mA cm⁻². On the contrary, as the applied current density is 30 mA cm⁻², the relatively smooth morphology is replaced with a relatively fine, star-like structure. The above improvement in morphology and adhesion in comparison with Figs. 3e and 4e strongly suggests that the dendrite formation can be suppressed

by adding PEG and that achieving a smoother film due to the PEG adsorption becomes more obvious at a higher current density of deposition.

In Fig. 4c and g, the Bi deposits plated from the solution with the gelatin additives show smoother surface morphologies than that plated from similar baths containing the PEG additives. This

Table 2

Summary of electroplating conditions from the plating solution containing 0.05 M Bi(NO₃)₃ and resultant properties of Bi deposits.

Compounds	Current density (mA cm ⁻²)	Adhesion	Avg. crystal size ^a (nm)
(a1) CA	1	Poor	–
(a2) CA	30	Poor	–
(b1) CA + PEG	1	Excellent	43.7
(b2) CA + PEG	30	Excellent	38.9
(c1) CA + gelatin	1	Poor	–
(c2) CA + gelatin	30	Poor	–
(d1) CA + PEG + gelatin	1	Excellent	38.1
(d2) CA + PEG + gelatin	30	Excellent	27.1
(e1) CA + EDTA	1	Very good	67.6
(e2) CA + EDTA	30	Poor	–
(f1) CA + EDTA + PEG	1	Very good	49.7
(f2) CA + EDTA + PEG	30	Very good	34.4
(g1) CA + EDTA + gelatin	1	Poor	–
(g2) CA + EDTA + gelatin	30	Poor	–
(h1) CA + EDTA + PEG + gelatin	1	Very good	31.4
(h2) CA + EDTA + PEG + gelatin	30	Very good	29.8

CA: citric acid, 0.3 M. EDTA: ethylenediaminetetraacetic acid, 0.05 M. PEG: polyethylene glycol (MW 400), 0.2 M. Gelatin: 4000 ppm.

^a The average crystal size is estimated from the XRD peak with the highest intensity.

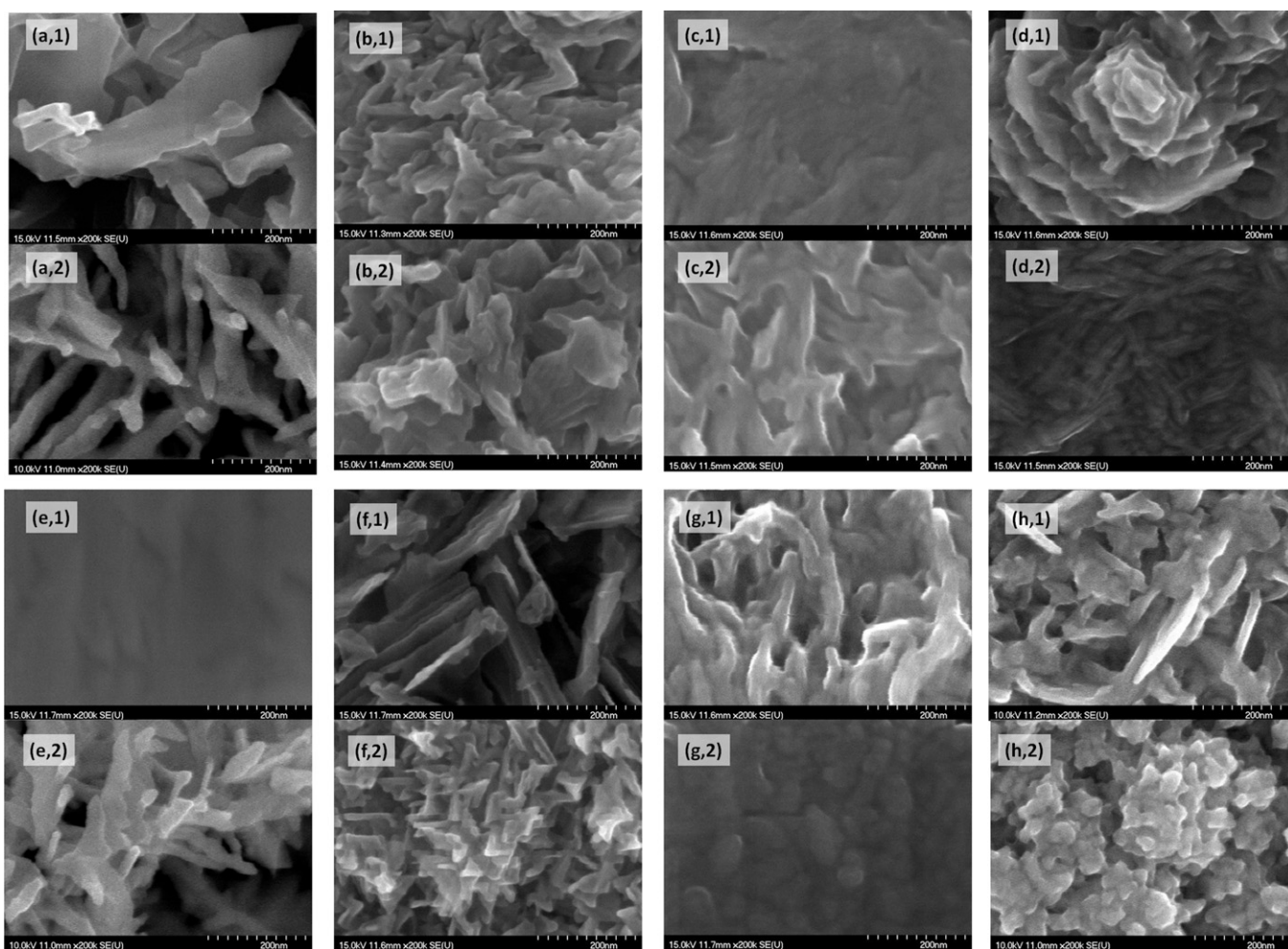


Fig. 4. SEM morphologies under a magnification of 200,000 for Bi deposits plated at (1) 1 and (2) 30 mA cm⁻² from the basic plating bath (0.05 M Bi(NO₃)₃) with (a) 0.3 M CA, (b) 0.3 M CA + 0.2 M PEG, (c) 0.3 M CA + 4000 ppm gelatin, (d) 0.3 M CA + 0.2 M PEG + 4000 ppm gelatin, (e) 0.3 M CA + 0.3 M EDTA, (f) 0.3 M CA + 0.3 M EDTA + 0.2 M PEG, (g) 0.3 M CA + 0.3 M EDTA + 4000 ppm gelatin, and (h) 0.3 M CA + 0.3 M EDTA + 0.2 M PEG + 4000 ppm gelatin.

result also indicates a strong adsorption effect of gelatin on the surface of Bi deposit. However, both Bi films show a poor adhesion property, full of cracks (see Fig. 3c and g), probably due to the formation of gelatin microspheres which tend to adhere together and can be considered as a compact shielding layer [24]. Since inhibition of the HER by the gelatin adsorption is weaker in comparison with PEG (see Figs. 1 and 2), hydrogen bubbles should extensively evolve at the boundaries of these compact shielding microspheres during electroplating, resulting in the formation of deep cracks. In Figs. 3d and 4d, the Bi deposits plated from the solution containing CA, PEG, and gelatin show very smooth surface morphologies and relatively smaller grains in different microstructures, such as flower-like or stitch-like, are homogeneously distributed on the deposits by varying the plating current density. This result strongly displays a synergistic adsorption effect of the mixed additives (i.e., a thin PEG–gelatin layer) on the deposits. In addition, in comparison with the deposits shown in Fig. 3c, the better adhesion of these deposits is attributed to the physical interaction between PEG and gelatin, decreasing the tendency to form a compact shielding layer of gelatin microspheres. This phenomenon should avoid the much localized hydrogen evolution on the deposit and consequently, the binary additives effectively avoid the formation of cracks. A similar synergistic effect is also visible in Figs. 3h and 4h which show the stitch-like and sphere-like morphologies with very good adhesion when the current densities of electroplating are equal to 1 and 30 mA cm⁻², respectively. Based on all the above results and dis-

cussion, the deposits plated from the baths containing unitary and binary additives (i.e., PEG, gelatin, or PEG–gelatin) show smoother morphologies in comparison with their counterparts especially under the plating current density of 30 mA cm⁻².

Fig. 5 shows the XRD patterns of the deposits with the crystalline structure, indicated in Table 2. From Table 2 and Fig. 5, the deposits with good adhesion generally show obvious diffraction peaks on their XRD patterns. An examination of these XRD patterns reveals that the preferred orientation of Bi deposits is significantly affected by varying the combination of complex and additives. For example, the (0 1 2) face is the preferred orientation for the deposits plated from the bath containing CA and PEG, which is independent of the plating current density (see curves 1 and 2). When gelatin was added into the above bath, this crystal face is significantly depressed when the current density was increased from 1 to 30 mA cm⁻² and the (1 1 0) face becomes the preferred orientation (see curves 3 and 4). For the deposits plated from the bath containing CA, EDTA, and PEG (see curves 5 and 6), the diffraction intensities of all peaks are low although the intensity of the (0 1 2) face is the highest. A similar phenomenon is also visible for the deposits plated from the bath containing CA, EDTA, PEG, and gelatin (see curves 7 and 8) while the preferred orientation is slightly changed by varying the current density of deposition. On curve 9, the deposit plated at 1 mA cm⁻² from the bath containing both CA and EDTA shows a polycrystalline structure with an excellent crystalline quality. This result supports the statement that

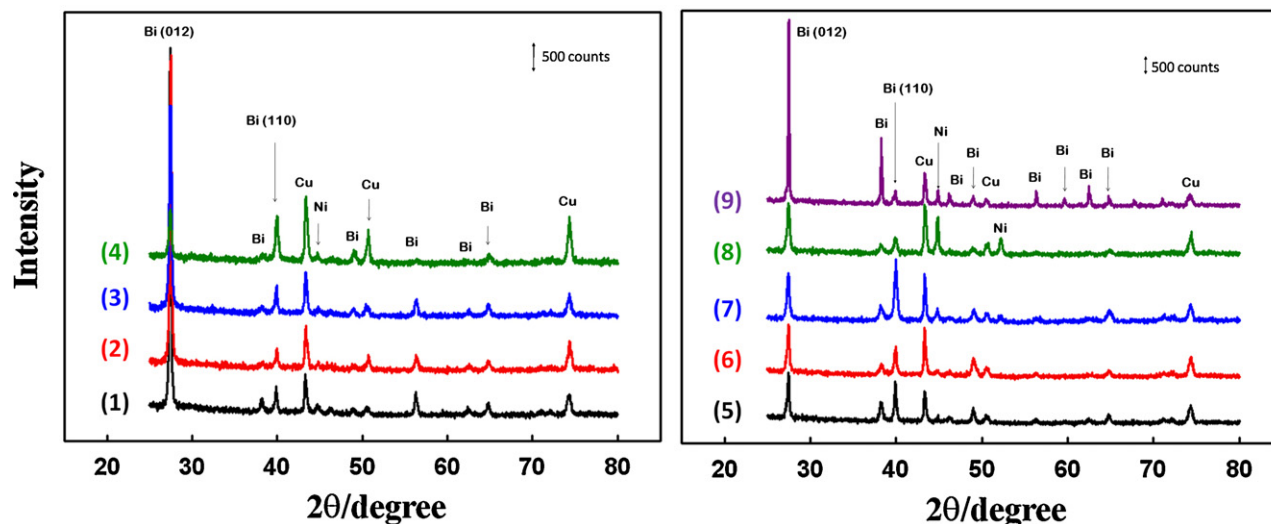


Fig. 5. XRD patterns of Bi deposits with good adhesion property plated from the basic plating bath with (1) 0.3 M CA + 0.2 M PEG, at 1 mA cm^{-2} , (2) 0.3 M CA + 0.2 M PEG, at 30 mA cm^{-2} , (3) 0.3 M CA + 0.2 M PEG + 4000 ppm gelatin, at 1 mA cm^{-2} ; (4) 0.3 M CA + 0.2 M PEG + 4000 ppm gelatin, at 30 mA cm^{-2} ; (5) 0.3 M CA + 0.3 M EDTA + 0.2 M PEG, at 1 mA cm^{-2} , (6) 0.3 M CA + 0.3 M EDTA + 0.2 M PEG, at 30 mA cm^{-2} ; (7) 0.3 M CA + 0.3 M EDTA + 0.2 M PEG + 4000 ppm gelatin, at 1 mA cm^{-2} , (8) 0.3 M CA + 0.3 M EDTA + 0.2 M PEG + 4000 ppm gelatin, at 30 mA cm^{-2} , and (9) 0.3 M CA + 0.3 M EDTA, at 1 mA cm^{-2} .

under this low deposition current density, the stacking of Bi atoms belongs to the pyramidal growth and a steady growth of Bi crystals [27,28]. Based on the full width at half-maximum (FWHM) method, the average crystal size of the Bi deposits was estimated from the strongest peak on all XRD patterns. These results are shown in Table 2. Obviously, the crystal size of Bi deposits plated from the same bath is larger when the current density of deposition is lower, reasonably due to a longer time and more opportunities for the surface movement of Bi ad-atoms freshly deposited on the surface of Bi grains. Accordingly, the crystalline quality and size of Bi are improved.

3.3. Sn^{2+} sensing by means of the SWASV analysis

This section tries to demonstrate the influences of certain physicochemical properties such as morphology and crystal size of Bi deposits (i.e., BFEs) on their sensing ability of Sn^{2+} ions. Here, five Bi deposits with their crystal size ~ 68 , ~ 39 , ~ 34 , ~ 30 , and ~ 27 nm were tested for this purpose. Since the background responses of BFEs in the stripping solution are very important to the sensing performances, the SWASV curves for the above five BFEs as well as the Ni/Cu substrate and a BFE pre-deposited with Sn are shown in Fig. 6a. From curve 6 in Fig. 6a, Ni starts to be oxidized at about -200 mV and a peak centered at 20 mV is found. For BFEs, their distinct stripping potential window can be set from ca. -300 to 0 mV with a peak centered at -80 mV to avoid the possible interference from Ni stripping although the difference between curves 1 and 6 is relatively unobvious. On the other hand, this effect shows no influence on the Sn^{2+} sensing since on curve 7, the potential window for anodic stripping of Sn is from ca. -600 to -300 mV with a peak at -480 mV. From all the above results and discussion, the SWASV curves for the anodic stripping of Sn have to be measured from -600 to -300 mV to avoid any stripping current from other possible metals such as Bi or Ni.

Typical SWASV results for Sn^{2+} sensing on the five BFEs with their Bi crystal size ~ 68 , ~ 39 , ~ 34 , ~ 30 , and ~ 27 nm are shown in Fig. 6b as curves 1–5, respectively. Clearly, curves 3–5 show the anodic stripping responses of Sn atoms which were previously accumulated onto the BFEs at -0.8 V for 300 s from the testing solution containing 35.4 ppm Sn^{2+} under a magnetic stirring rate of 100 rpm . On the other hand, the order of the SWASV curves with respect to increasing their peak current density, centered

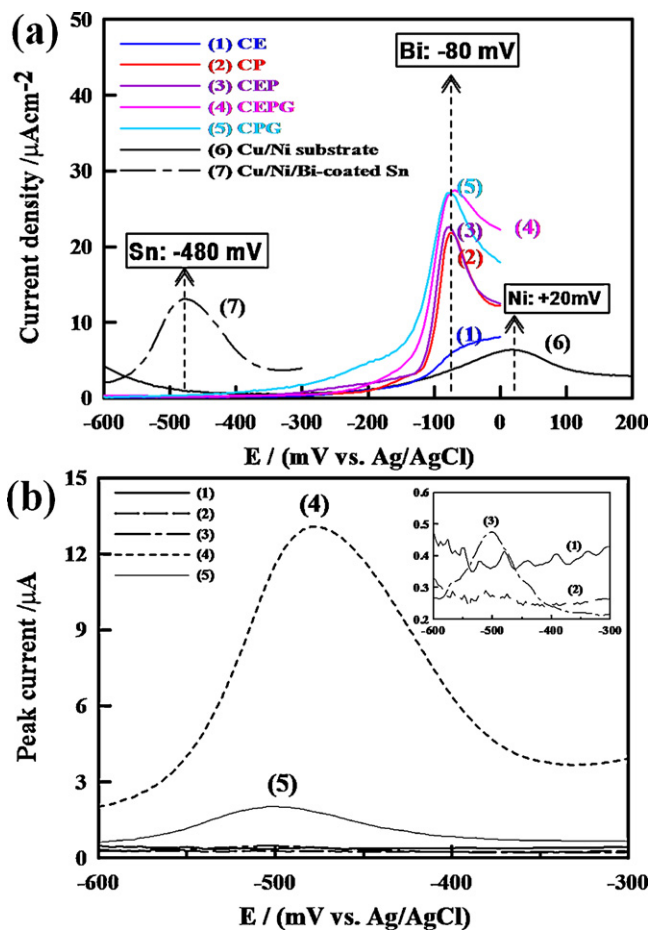


Fig. 6. The SWASV curves measured in 0.1 M citric acid for Bi deposits, (a) without and (b) with Sn pre-deposition, prepared from the basic plating bath with (1) $0.3 \text{ M CA} + 0.3 \text{ M EDTA}$, at 1 mA cm^{-2} , (2) $0.3 \text{ M CA} + 0.2 \text{ M PEG}$, at 30 mA cm^{-2} , (3) $0.3 \text{ M CA} + 0.3 \text{ M EDTA} + 0.2 \text{ M PEG}$, at 30 mA cm^{-2} , (4) $0.3 \text{ M CA} + 0.3 \text{ M EDTA} + 0.2 \text{ M PEG} + 4000 \text{ ppm gelatin}$, at 30 mA cm^{-2} , and (5) $0.3 \text{ M CA} + 0.2 \text{ M PEG} + 4000 \text{ ppm gelatin}$, at 30 mA cm^{-2} . The cathodic pre-deposition of Sn on BFEs is carried out at -0.8 V for 300 s from a 0.1 M CA solution containing 35.4 ppm Sn^{2+} . Curve 6 in (a) is the SWASV response of Ni/Cu and curve 7 is the SWASV response of curve 4 in (b).

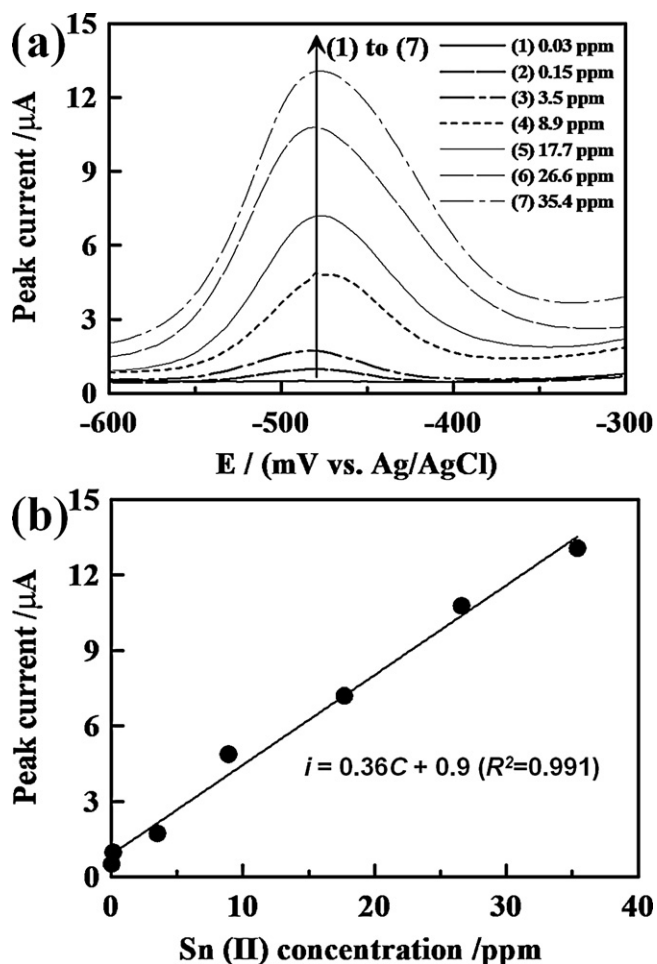


Fig. 7. The SWASV curves measured in 0.1 M citric acid for the Bi deposit plated from the basic plating bath with 0.3 M CA + 0.3 M EDTA + 0.2 M PEG + 4000 ppm gelatin at 30 mA cm⁻². (a) The cathodic pre-concentration of Sn on the BFEs is carried out at -0.8 V for 300 s from a 0.1 M CA solution containing (1) 0.03, (2) 0.15, (3) 3.5, (4) 8.9, (5) 17.7, (6) 26.6, and (7) 35.4 ppm Sn²⁺. (b) The calibration plot for the SWASV peak current against the Sn²⁺ concentration.

around -480 mV, is: curve 3 (0.48 µA) < curve 5 (2.03 µA) < curve 4 (13.08 µA) meanwhile no detectable information is found on curves 1 and 2. These results reveal that the sensing ability of BFEs is significantly influenced by the crystal size and morphology of Bi deposits. In addition, the smaller nano-sized crystal and porous morphology of a Bi deposit are, the better sensitivity for Sn²⁺ detection can be obtained, suggesting that the amount of Sn previously depositing on the Bi deposits depends on the active surface area of the Bi deposits.

Since the BFE deposited at 30 mA cm⁻² from the bath containing 0.3 M CA, 0.3 M EDTA, 0.2 M PEG, and 4000 ppm gelatin shows the highest sensitivity in the testing solution, the sensing ability of this deposit is further examined by changing the Sn²⁺ concentration in the testing solution. Typical results are shown in Fig. 7a and the plot for the peak current density against the concentration of Sn²⁺ is shown in Fig. 7b. Clearly, Fig. 7b displays a linear relationship between the peak current density and the concentration of Sn²⁺. This linear dependence of peak current density on the concentration of Sn²⁺ can be perfectly fitted by the following equation:

$$i = 0.36C + 0.9 \quad (R^2 = 0.991)$$

where i and C indicate the peak current (in µA) and Sn²⁺ concentration (in ppm), respectively. Since the regression coefficient, R^2 ,

is close to 1, the concentration of Sn²⁺ from 0.15 to 35.4 ppm can be precisely determined by the SWASV method. The above results reveal that BFEs with small nanocrystals and a porous morphology will be a good electrochemical sensors for detecting trace Sn²⁺. The optimization of BFEs for detecting trace Sn²⁺ and the other heavy metal ions is going to be carried out very recently in this lab.

4. Conclusions

Based on the LSV analyses, the deposition behavior of Bi³⁺ ions in the plating bath containing various combinations of complex agents and additives can be understood. PEG and gelatin mainly work as a leveling agent adsorbed on the surface of Bi deposits. From the SEM images, PEG improves the adhesion and suppresses the formation of dendrites for Bi deposits, resulting in a smoother film. On the contrary, the formation of a compact shielding layer of gelatin microspheres leads to localized hydrogen evolution on the deposit and deeply cracked deposits with poor adhesion are obtained. The binary PEG-gelatin additives avoid the above phenomenon and favor to form sphere-like Bi nanocrystals with a porous morphology at a high current density of deposition (30 mA cm⁻²). The morphology and crystal size (from 27 to 68 nm) of Bi deposits can be controlled by varying the combination of CA, EDTA, PEG, and gelatin as well as the current density. From the SWASV results, the deposit with a smaller crystal size and a porous morphology exhibits the excellent sensitive ability to Sn²⁺ with a limiting detection concentration of 0.15 ppm.

Acknowledgments

The financial support of this work by the National Science Council of ROC, Taiwan and the boost program of NTHU, is gratefully acknowledged.

References

- [1] X. Liu, P. Sun, S. Ren, L. Wen, *Electrochem. Commun.* 10 (2008) 136.
- [2] E. Hutton, B. Ogorevc, S. Hoever, F. Weldon, M. Smyth, J. Wang, *Electrochem. Commun.* 3 (2001) 707.
- [3] K. Takamura, H. Shimamura, N. Koshiba, Thin film for package of alkaline battery and thin air battery using the same, Google Patents (2005).
- [4] F. Yang, K. Liu, C. Chien, P. Searson, *Phys. Rev. Lett.* 82 (1999) 3328.
- [5] F. Yang, K. Liu, K. Hong, D. Reich, P. Searson, C. Chien, *Science* 284 (1999) 1335.
- [6] B. Popov, R. White, G. Zheng, *Corrosion* 51 (1995) 429.
- [7] R. Kachooangi, C. Banks, X. Ji, R. Compton, *Anal. Sci.* 23 (2007) 283.
- [8] F. Arduini, J.Q. Calvo, G. Palleschi, D. Moscone, A. Amine, *TrAC-Trends Anal. Chem.* 29 (2010) 1295.
- [9] X. Duan, J. Yang, W. Zhu, X. Fan, C. Xiao, *Mater. Lett.* 61 (2007) 4341.
- [10] S. Jiang, Y. Huang, F. Luo, N. Du, C. Yan, *Inorg. Chem. Commun.* 6 (2003) 781.
- [11] L. Li, Y. Zhang, G. Li, X. Wang, L. Zhang, *Mater. Lett.* 59 (2005) 1223.
- [12] D. Beutler, N. Giordano, *Phys. Rev. B* 38 (1988) 8.
- [13] D. Kim, S. Lee, J. Kim, G. Lee, *Appl. Surf. Sci.* 252 (2006) 3525.
- [14] S. Cho, Y. Kim, A. Freeman, G. Wong, J. Ketterson, L. Olafsen, I. Vurgaftman, J. Meyer, C. Hoffman, *Appl. Phys. Lett.* 79 (2001) 3651.
- [15] Y.-D. Tsai, C.-C. Hu, C.-C. Lin, *Electrochim. Acta* 53 (2007) 2040.
- [16] Y.-D. Tsai, C.-C. Hu, *J. Electrochem. Soc.* 156 (2009) D58.
- [17] Y.-D. Tsai, C.-C. Hu, *J. Electrochem. Soc.* 156 (2009) D490.
- [18] C.-C. Hu, Y.-D. Tsai, C.-C. Lin, G.-L. Lee, S.-W. Chen, T.-C. Lee, T.-C. Wen, *J. Alloys Compd.* 472 (2009) 121.
- [19] C.-C. Hu, G.-L. Lee, *J. Chin. Inst. Eng.* 37 (2006) 589.
- [20] L. Bonou, M. Eyraud, R. Denoyel, Y. Massiani, *Electrochim. Acta* 47 (2002) 4139.
- [21] W. Dow, H. Huang, M. Yen, H. Huang, *J. Electrochem. Soc.* 152 (2005) C425.
- [22] S. Wen, J. Szpunar, *Electrochim. Acta* 50 (2005) 2393.
- [23] T. Pal, A. Ganguly, D. Maity, *Bull. Chem. Soc. Jpn.* 60 (1987) 3001.
- [24] S. Derkatch, L. Petrova, V. Izmailova, B. Tarasevitch, *Colloids Surf. A* 152 (1999) 189.
- [25] H. Thakkar, R. Murthy, *ARS Pharmaceutica* 46 (2005) 19.
- [26] T. Kushibiki, H. Matsuoka, Y. Tabata, *Biomacromolecules* 5 (2004) 202.
- [27] F. Walsh, M. Herron, *J. Phys. D: Appl. Phys.* 24 (1991) 217.
- [28] L. Guo, P. Searson, *Electrochim. Acta* 55 (2010) 4086.
- [29] E. Sandnes, M. Williams, U. Bertocci, M. Vaudin, G. Stafford, *Electrochim. Acta* 52 (2007) 6221.